JTTEE5 11:95-99

Effect of Post-Heat Treatment on the Corrosion Resistance of NiWCrBSi HVOF Coatings in Chloride Solution

L. Gil, M.A. Prato, and M.H. Staia

(Received 21 June 2000; in revised form 22 November 2000)

High velocity oxygen fuel (HVOF) thermal spray is one of the most versatile and fastest techniques used to apply wear- and corrosion-resistant coatings to critical component surfaces. In such applications where the material is submitted to a corrosive environment, coating porosity is one of the most important microstructural aspects determining the performance of the material. In the present work, the results regarding the effect of both carburizing flame and argon atmosphere post-heat treatments on the microstructure and corrosion resistance of NiCrWBSi coatings are reported. Both microstructural characterization and porosity determination were carried out before and after the heat treatments. It was determined that both treatments had reduced the porosity considerably, and this reduction was accompanied by pronounced microstructural changes regarding the disappearance of the initial lamellar structure, a more uniform distribution of the hard phases, and a decrease in the number of microcracks and unmelted particles. Results from potentiodynamic studies carried out in a 5% NaCl solution have indicated an increase in the corrosion resistance of both heat-treated coatings.

Keywords corrosion, HVOF, Ni-based coating, post-heat treatment

1. Introduction

Coatings obtained by thermal spray technology are widely used in many industrial applications where abrasion wear and corrosion resistances are required. Because of inherent processing characteristics, thermal spray coatings present microporosity, microcracks, oxides, and unmelted particles which influence the mechanical properties and seriously compromise their corrosion resistance in a given environment.[1-3]

Several studies[4,5] have demonstrated that coating porosity acts like a crevice, inducing crevice corrosion, and that severe galvanic corrosion will occur if the electrolyte reaches the substrate for coatings that are nobler (i.e., cathodic to the substrate).

Although the development of higher velocity processes (e.g., high velocity oxygen fuel [HVOF] and D-Gun) has contributed to a decrease in the coating porosity, the transport of the corrosive species could only be impeded by different post-treatments that can be applied to the as-deposited coatings. Different techniques such as flame, plasma jet, laser, isostatic hot pressing, and atmospheric and vacuum furnace heating[1,2,4,6-9] have been successfully applied. Impregnation methods[10] also could be an alternative in diminishing the amount of the reactive surface and preventing the contact between the corrosive liquids and the substrate.

Nickel-based alloys, which incorporate fine hard phases such as borides, carbides, and carboborides distributed uniformly thorough the Ni-Cr-B matrix, have performed successfully against abrasion wear,[1,2] but both the porosity and the moderate adhesion of the coating are the main concerns when corrosion resistance is required.

Therefore, the present work was performed with the aim of determining the influence of the post-heat treatment on the corrosion behavior and microstructure of an HVOF nickel-based alloy.

2. Experimental Procedure

HVOF was carried out using a Hobart Tafa JP-5000 (USA) gun on an AISI 1020 substrate. The substrate material was grit blasted by using angular chilled iron prior to thermal spraying. The nominal composition of the commercial NiWCrBSi alloy is presented in Table 1.

The nickel-based alloy powders employed had a particle size range of 22 to 63 μm[3] and presented an equivalent diameter of 31.45 μm. Table 2 summarizes the deposition conditions for HVOF. The final coating thickness for all samples was controlled to be 0.3 mm.

The as-deposited samples were post-heat treated by using

Table 1 Nominal Composition of Nickel Alloy (Colmonoy 88)

	W	Cr	B	Fe	Si	C	Ni
wt.%	17.00	15.00	3.00	3.50	4.00	0.75	Balance

L. Gil, Department of Metallurgical Engineering, National Polytechnic University (UNEXPO), Puerto Ordaz, Estado Bolivar, Venezuela; **M.A. Prato,** School of Mechanical Engineering, Central University of Venezuela, Caracas, Venezuela; and **M.H. Staia,** School of Metallurgical Engineering and Materials Science, Central University of Venezuela, Apartado 49141, Caracas 1042-A, Venezuela. Contact e-mail: mstaia@mailserver.reacciun.ve.

Table 2 HVOF Thermal Spray Process Conditions

Gun	JP-5000
Barrel length	100 mm
Kerosene flow	0.38 l/min
Kerosene pressure	1.17 MPa
Oxygen flow	0.80 l/min
Combustion chamber pressure	0.82 MPa
Powder feed rate	0.091 kg/min
Nitrogen flow as carrier	14 l/min
Spray distance	330 mm

both oxyacetylene flame and the standard furnace heating in argon. The torch treatment was performed manually until a shiny glaze was obtained at the surface of the coatings. The conditions employed for the furnace heat treatment, which were based on those of previous experiments[2,11] are shown in Fig. 1.

Microstructure and morphology of both the as-deposited and the heat-treated coatings were examined by using an optical and a scanning electron microscope (SEM, Philips Model XL30, The Netherlands) with an x-ray energy-dispersive system (EDS, EDAX DX4, USA). Samples were sectioned with a low-speed diamond saw. After vacuum impregnation and cold epoxy mounting, the cross-sections were metallographically prepared with a 0.05 silica colloidal polishing medium. SEM examinations also were carried out on the corroded surface of the coatings after testing to further understand the corrosion behavior. Porosity measurements were performed by using quantitative image analysis on the polished cross-sections of all samples. The reported Vickers microhardness (HV_{300}) values were based on the average value of 10 readings on the coating surface.

The corrosion behavior of coatings was evaluated by employing an anodic polarization method that was performed according to ASTM G5-94 guidelines in a deaired 3.5% NaCl solution. A potentiostat (EG&G model 273A, USA) was used with a potential range of between −0.25 and 1 V, and a scan rate of 1 mV/s. In order to activate the surface, before polarization, the samples were cathodically cleaned for 5 min at –0.400 mV below the value corresponding to the open circuit potential.

3. Results and Discussion

3.1 Microstructural Characterization of As-Deposited and Heat-Treated Coatings

The typical structure of as-sprayed coatings is shown in Fig. 2, which is an SEM micrograph that was obtained in backscatter mode (BS), in which a lamellar morphology with unmelted particles is observed. High microporosity can be noticed between the lamella and the unmelted particles. The hard phases are not uniformly distributed and display different morphologies ranging from angular to round-shaped. The regions that correspond to the darker and lighter areas, containing the hard phases, have been analyzed by an EDS, which indicated the presence of a nickel-based metal matrix with different composition (i.e., a multicomponent eutectic in the Ni-Cr-Fe-B-Si system).

SEM micrographs (BS mode) corresponding to the cross-sections of the as-sprayed and heat-treated coatings are presented in Fig. 3 for comparison. It can be noticed that both heat treatment methods reduced the porosity and the number of microcracks and unmelted particles. The lamellar structure, which is characteristic of the as-deposited coating, has disappeared, and the hard phases are more uniformly distributed in the matrix. Figure 4 shows the coating-substrate interface for the furnace and the torch heat-treated coatings. As could be observed, the furnace heat-treated coating (Fig. 4b), contrary to the torch heat-treated coating (Fig. 4a), presents a heat-affected zone of ~9 mm. This is an indication of the formation of a metallurgical bond between the coating and substrate in this instance. The diffusion process, which has occurred for furnace heat-treated coatings, will assure a better bond between the coating and substrate.

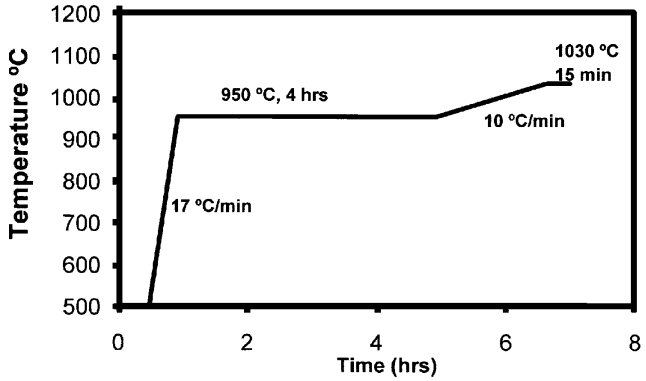

Fig. 1 Experimental conditions employed for the heat treatment of samples in an argon atmosphere

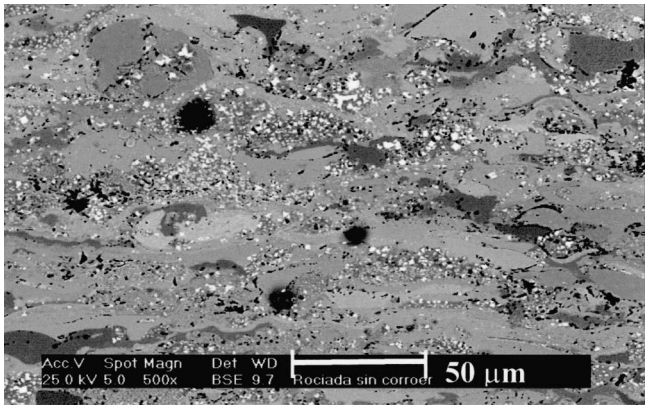

Fig. 2 SEM micrograph (BS mode) showing the typical structure of as-sprayed coatings

3.2 Microhardness

Microhardness values of an average of 539 ± 34 HV_{300} was measured for the as- sprayed coatings. For flame-treated and furnace-treated coatings, microhardness values of 686 ± 56 HV_{300} and 656 ± 44 HV_{300}, respectively, were obtained. These latter values show an increase of 25% when compared to the microhardness values obtained for the as-sprayed coatings, representing the consequence of the homogenous distribution of hard phases and a decrease of both the porosity and the number of unmelted particles induced by heat treatment.

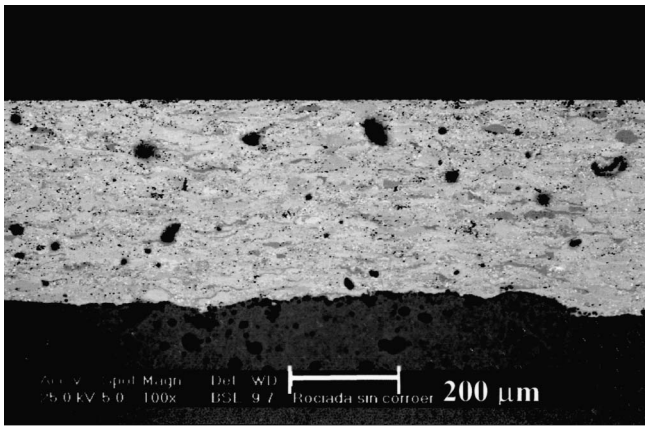

(a)

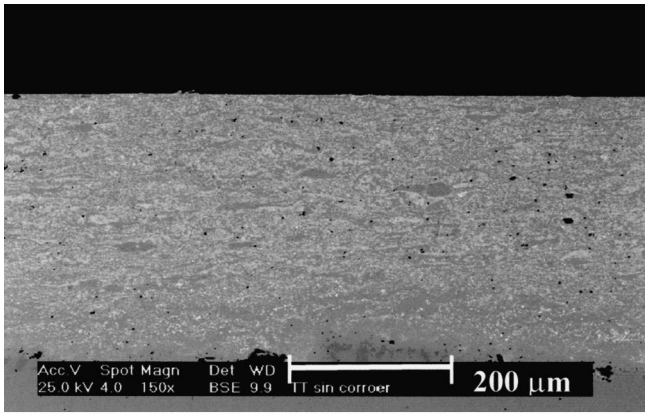

(b)

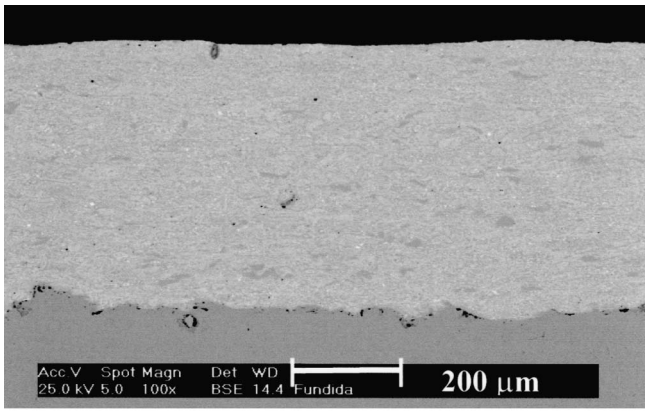

(c)

Fig. 3 SEM micrographs (BS mode) of **(a)** the as-sprayed coating, **(b)** the furnace heat-treated coating, and **(c)** the torch-treated coating

3.3 Corrosion Results

The typical polarization curves for the as-sprayed coating and the heat-treated coating is shown in Fig. 5. For comparison, the polarization curve corresponding to the steel substrate also is included. As can be observed, a small passivation was obtained only for the furnace heat-treated samples, and this tendency disappeared as the potential was increased.

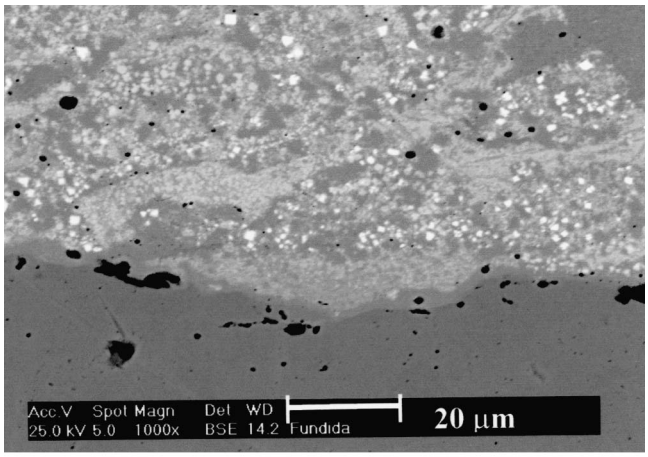

(a)

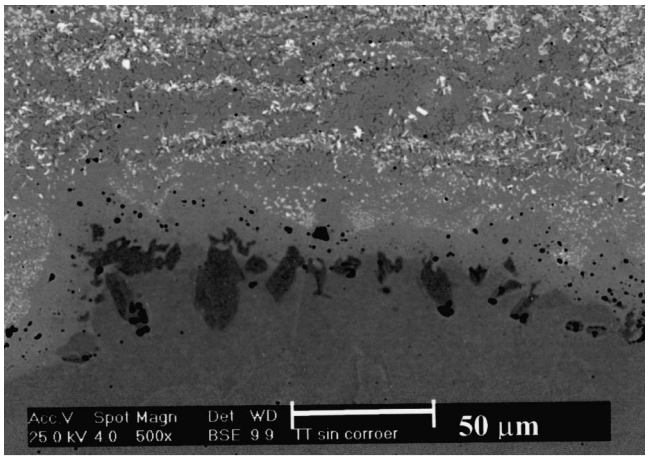

(b)

Fig. 4 SEM micrographs (BS mode) of the coating-substrate interface **(a)** for torch treatment and **(b)** for furnace treatment

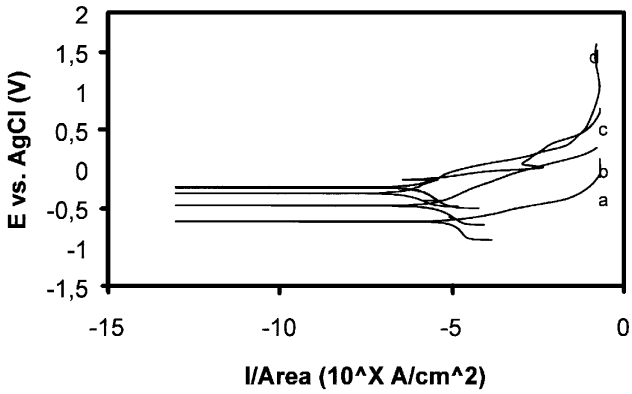

Fig. 5 Typical polarization curves in a 5% Na Cl solution of **(a)** steel AISI 1020; **(b)** the as-sprayed coating, **(c)** the flame-treated coating, and **(d)** the furnace-treated coating

The results from the corrosion experiments are shown in Table 3, where data regarding the coating porosities also have been included. The values obtained for the corrosion potential

Table 3 Experimental Results for Samples Under Study

Sample	Porosity, %	E_{corr}, V	i_{corr}, μA.cm^{-2}
Steel 1020	—	−0,68	10,77
As-sprayed coating	2.05	−0,47	3,62
Flame treated	0.08	−0,26	0,88
Furnace treated	0.10	−0,31	0,41

and corrosion current density for the 1020 AISI steel in a sodium chloride solution correspond to the literature data. As shown in Table 3, the corrosion current density has decreased 2.9 times in the as-sprayed condition compared to the substrate, indicating the beneficial effect of the coating. The corrosion current for both heat-treated coatings shows a decrease of 4.1 times and nearly one order of magnitude, respectively, for the torch and furnace heat treatments compared to as-sprayed coatings. As could be noticed, the initial porosity of the as-sprayed coating of 2.05% has significantly decreased after heat treatment, reaching 0.08% for torch treatment and 0.1% for the samples that have been heat treated in argon.

The morphologies of the corrosion products are presented in Fig. 6. EDS performed on the area indicated the presence of Cr (20.46 at.%) and Ni (42.42 at.%) for the as-deposited sample. For the flame heat-treated samples, EDS analysis of the corrosion products has indicated the presence of O (30.94 at.%), W (9.66 at.%), Cr (47.24 at.%), Ni (10.50 at.%), and Fe (1.66 at.%). Meanwhile, for the samples treated in argon, the corrosion products presented a composition of O (36.3 at.%), W (24.15 at.%), Cr (24.42 at.%), Ni (12.45 at.%), and Fe (1.53 at.%).

Microstructural characterization of the corroded coatings could explain the observed behavior in the case of the as-sprayed coatings. An SEM micrograph (BS mode) of the cross-section of the corroded as-sprayed coating is shown in Fig. 7(a). EDS analysis performed at the coating-steel interface revealed the presence of iron oxide. The high value corresponding to the corrosion current density, I_{corr}, corroborates the presence of interconnected pores and microcracks between lamella, which have allowed the electrolyte penetration, causing a difference in aeration (i.e., crevice corrosion) and galvanic corrosion between the coating and the substrate. An increased dissolution of the matrix is indicated by the dark area in Fig. 7(a), which is due to the microgalvanic cells formed between the hard phases, which are nobler than the nickel matrix, and the matrix. EDS analysis performed in this area indicated the presence of 26 at.% of O_2 and 39.5 at.% of Na.

Figure 7(b) shows the SEM micrograph (BS mode) of the cross-section of a corroded coating that has been furnace heat treated. Here, the matrix dissolution can also be noticed. However, it was observed that, in this case, the electrolyte does not reach the coating-substrate interface, indicating the effectiveness of post-heat treatment in sealing and decreasing the interconnecting paths to the substrate.

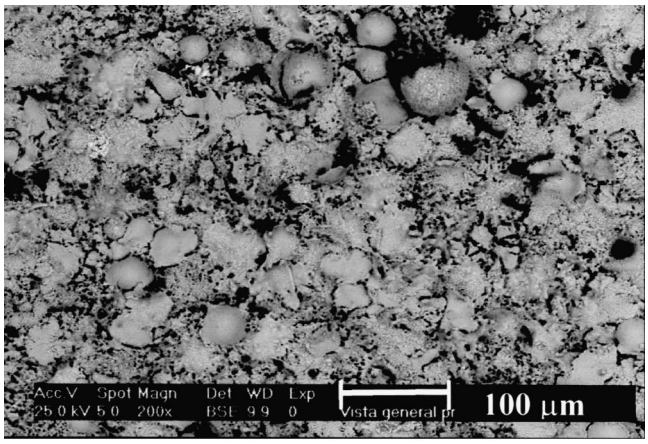

(a)

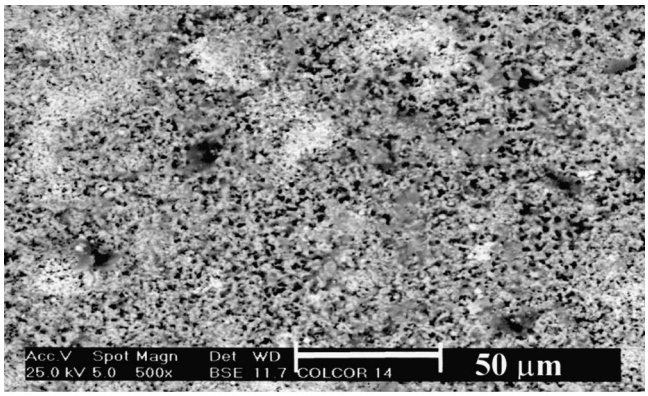

(b)

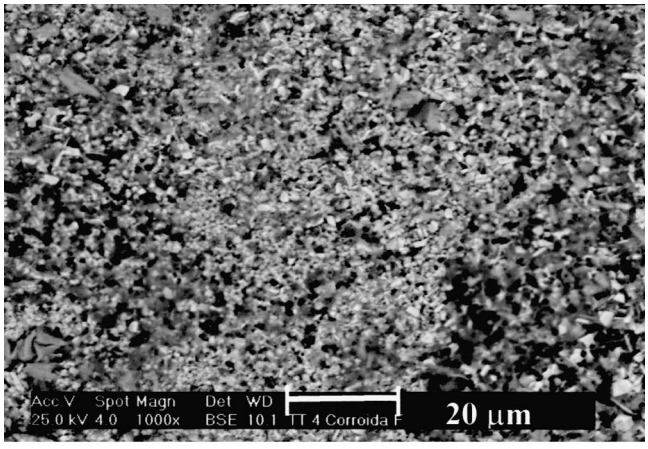

(c)

Fig. 6 SEM micrographs (BS mode) of the morphologies of the corrosion products of **(a)** the corroded as-sprayed NiWCrBSi coating, **(b)** the flame-treated coating, and (**c**) the furnace-treated coating

4. Conclusions

The present investigation has shown that postcoating heat treatments have substantially altered the structure of deposits by decreasing the porosity and increasing both the density and surface hardness. In the case of the coatings that were heat treated in argon, an improvement of the metallurgical bond between the deposits and the substrate also was achieved. The post-heat treatments have improved the corrosion resistance of the coating-substrate system by decreasing the amount of heterogeneities of the as-sprayed HVOF coatings such as porosity and mi-

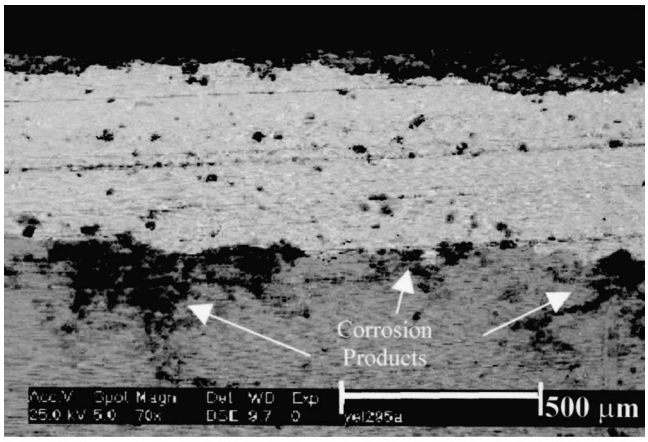

(a)

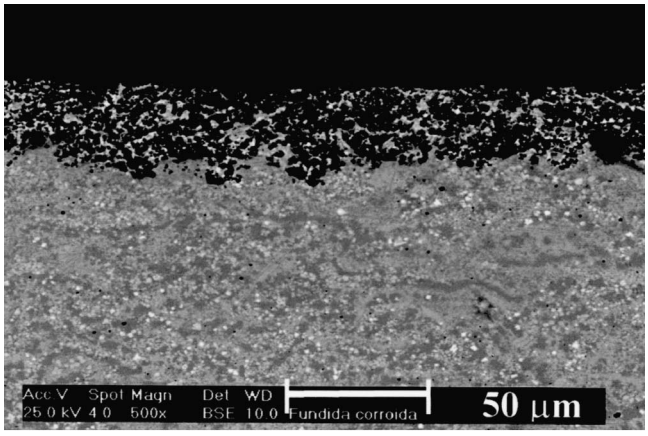

(b)

Fig. 7 SEM micrographs of the cross-sections of the corroded samples: **(a)** the as-deposited coating; and **(b)** the furnace-treated coating

crocracks between lamella, which act as pathways between the substrate and the environment. The presence in the microstructure of nobler species such as carbides and borides, although they enhance mechanical properties such as hardness, also generate microgalvanic corrosion.

It was shown that the torch heat treatment process is quite effective in improving corrosion resistance. However, this process depends largely on the experience of the operator, which leads to low reproducibility.

The potentiodynamic polarization test can be used as a quick indicator of coating quality and corrosion resistance in a specific environment. This test could contribute to the optimization of the coating quality, and it can be included in the procedures of quality assurance to support the information obtained by other control procedures.

Acknowledgments

The authors acknowledge the financial support of the National Council for Scientific and Technological Research of Venezuela (CONICIT), through projects S1-96001366 and LAB -9700644, and the Council for Scientific and Humanistic Development (CDCH) of the Central University of Venezuela.

References

1. D.Z. Guo, F.L. Li, J.Y. Wang , and J.S. Sun: "Effects of the Post Coating Process on Structure and Erosive Wear Characteristics of Flame and Plasma Spray Coatings," *Surface Coatings Technol.*, 1995, *73*, pp. 73-78.
2. Y.H. Shieh , J.T. Wang, H. Shih, and S. Wu: "Alloying and Post Heat Treatment of Thermal Sprayed Coating of Self Fluxing Alloys," *Surface Coatings Technol.*, 1993, *58,* 1993, pp. 73-77.
3. L. Gil and M.H. Staia: "Microstructure and Properties of the HVOF Thermal Sprayed NiWCrBSi Coatings," *Surface Coatings Technol.*, 1999, *120-121*, pp. 423-29.
4. L. Fillion: "New Developments in Nickel-Based Self Fluxing Alloys," in *Thermal Spray: Research, Design and Application*, C.C. Berndt and T.F. Bernecki, ed., ASM International, Materials Park, OH, 1993, pp. 365-68.
5. C. Eminoglu, R. Knight, J. De Falco, and M. Dorfman: "Potentiodynamic Corrosion Testing of HVOF Sprayed Stainless Steel Alloy," in *Tagungsband Conference Proceedings*, E. Lugscheider and P.A. Kammer, ed., DVS Deutscher Verband fur Schweiβen, Dusseldorf, Germany, 1999, pp. 39-44.
6. C.C. Lim, S.C. Lim, M.O. Lai, and S.F. Chong: "Annealing of Plasma Sprayed WC-Co Coatings," *Surface Coatings Technol.*, 1996, *79*, pp. 151-61.
7. S. Du Bois: *Hard Surfacing Alloy with Precipitated Metal Carbides and Process*, U.S. Patent 5,387,294, Feb. 7, 1995.
8. A. Petibon, L. Bouquet, and D. Delsart: "Laser Surface Sealing and Strengthening of Zirconia Coatings," *Surface Coatings Technol.*, 1991, *49*, pp. 57-61.
9. K.A. Khor: "Hot Isostatic Pressing Modifications of Pores Size Distribution in Plasma Sprayed Coatings," *Mater. Manuf. Process*., 1997, *12*(2), pp. 291-307.
10. J. Knuuttila, P. Sorsa, and T. Mäntylä: "Sealing of Thermal Spray Coatings by Impregnation, *J Thermal Spray Technol.*, 1999, *8*(2), pp. 249-57.
11. M. Rodriguez, M.H. Staia, L. Gil, F. Arenas, and A. Scagni: "Study of the Influence of the Post Heat Treatment on the Properties of a High Velocity Oxyfuel (HVOF) Thermal Sprayed Ni Based Alloy," in *Advances in Science and Technology 20: Surface Engineering*, P. Vincenzini, ed., Techna, Faenza, Italy, 1999, pp. 479-83.